Characterization of Conformational Changes Coupled to Ligand Photodissociation from the Heme Binding Domain of FixL†

Jaroslava Mikšovská,‡ Christine Suquet,§ James D. Satterlee,§ and Randy W. Larsen*,‡

Department of Chemistry, University of South Florida, 4202 East Fowler Avenue SCA 400, Tampa, Florida 33620, and Department of Chemistry, Washington State University, P.O. Box 644630, Pullman, Washington 99164-4630

Received December 15, 2004; Revised Manuscript Received May 25, 2005

ABSTRACT: Using transient absorption spectroscopy and photoacoustic calorimetry (PAC), we have characterized carbon monoxide photodissociation and rebinding to two forms of the heme domain of *Bradyrhizobium japonicum* FixL. Transient absorption results for the complete heme domain (FixL residues 140−270) and a truncated heme domain (missing 11 residues on the N-teminal end and 14 amino acid residues on the C-terminal end of the full length heme domain) show similar rates for ligand rebinding to the five-coordinate heme domain and the absence of any transient intermediate on a microsecond time scale. Results from PAC studies show that both the truncated and complete heme domains undergo a contraction upon ligand photolysis. In addition, CO photolysis from the complete heme domain gives rise to an intermediate with a lifetime of ∼150 ns which is absent in the truncated heme domain. We attribute the 150 ns phase to ligand release to the solvent which may be accelerated in the case of the truncated domain. The initial contraction is attributed to changes in the charge distribution due to reorganization of the surface salt bridge formed between Glu182 and Arg227 or possibly to reorientation of Arg206. Changes in the charge distribution may play an important role in communication between the sensor domain and the regulatory domain and thus may be part of the signal transduction pathway.

Bacteria employ two-component sensing and signaling systems to constantly monitor changes in their surroundings and respond adequately to stimuli by alteration in development, virulence, location, or metabolism (*1*). In their simplest form, such signaling systems often consist of a sensor kinase with environmentally regulated catalytic phosphorylation activity and a response regulator with transcription stimulation activity. The activity of the response regulator is controlled by its phosphorylation status, and its activaton occurs when the sensor kinase catalyzes transfer of a phosphoryl group from ATP. The nitrogen-fixing bacteria, including *Bradyrhizobium japonicum* (*Bj*) and *Sinorhizobium meliloti* (*Sm*), formerly known as *Rhizobium meliloti* (*Rm*), contain a two-component oxygen sensing system composed of FixL and FixJ proteins that directly modulate expression of the fixK2 gene whose product is a transcriptional activator for a large group of genes involved with nitrogen fixation, denitrification, and anaerobic and microaerobic metabolism (*2*−*5*). Two different functional domains were identified in FixL, an N-terminal PAS heme domain and a histidine kinase domain at the C-terminal end (*6*−*8*). In its active state, the histidine kinase domain catalyzes phosphorylation of FixJ, its associated transcriptional regulator. In the absence of FixJ, autophosphorylation of FixL can occur. With a decreasing oxygen tension in the cell due to root growth and nodulation, oxygen dissociates from the heme domain, which activates phosphorylation by the C-terminal kinase domain, leading to transcription of the genes required for N_2 fixation (*7*, *8*).

The FixL heme domain (FixLH) contains a PAS-type fold that has been identified in more than 1000 signaling proteins (*9*−*11*). Crystal structures of FixLH from *B. japonicum* (*Bj*FixLH)[1] and *S. meliloti* (*Sm*FixLH) have been resolved and exhibit very similar structural features (*12*−*14*, *17*). In each, the sensor heme is held between five antiparallel β strands on the distal side and an α helix on the proximal side. His200 (*B. japonicum* nomenclature) within the α helix provides the proximal ligand for heme coordination. FixL−FixLH heme coordination and ligation were studied by UV−vis and resonance Raman spectroscopies (*15*, *16*), establishing the presence of high-spin, five-coordinate heme in the absence of exogenous ligands and low-spin, six-coordinate heme when appropriate ligands are present. On the basis of a comparison of the deoxy and oxy structures of *Bj*FixLH, one early mechanism for signal transduction was proposed (*13*) in which loss of heme-bound O_2 is accompanied by a heme Fe^{2+} spin-state change, concomitant geometry change, and alteration of heme planarity. The heme planarity changes alter peripheral hydrogen bonding between the heme propionates and F/G loop amino acids (residues Thr209−Arg220). A major feature of this mechanism is the significant movement of a distal amino acid, Arg220, which forms a

† We thank the American Heart Association (Grant 025537 to R.W.L.), the National Science Foundation (Grant MCB0317334 to R.W.L.), and the National Institutes of Health (Grant RO1 GM47645 to J.D.S.).

* To whom correspondence should be addressed. E-mail: rlarsen@cas.usf.edu. Phone: (813) 974-7925. Fax: (813) 974-3203.

‡ University of South Florida.

§ Washington State University.

[1] Abbreviations: *Bj*FixL, *B. japonicum* FixL; *Bj*FixLH, *B. japonicum* FixL heme domain; Fe(III)4SP, Fe tetrakis(4-sulfonatophenyl)porphine; PAC, photoacoustic calorimetry; PAS, Per-ARNT-Sim domain superfamily; TA, transient absorption spectroscopy.

10.1021/bi047369b CCC: $30.25
Published on Web 07/07/2005

salt bridge with propionate 7 in the unliganded structure, but rotates into the heme pocket to form a hydrogen bond with the heme-bound oxygen in oxy-*Bj*FixLH (*14*).

However, a more recent mechanistic proposal involves ligation-dependent structural rearrangements of selected distal amino acids. For example, Perutz and co-workers proposed that a "hydrophobic triad" composed of Ile209, Leu230, and Val232 (*S. meliloti* nomenclature) in the heme binding pocket may be involved in the sensing mechanism (*16*). Separately, on the basis of structural and spectroscopic characterization of *Sm*FixLH, Miyatake et al. (*17*) have proposed that steric repulsion between the bound oxygen molecule and Ile209 results in conformational changes in the F/G loop and that these changes may be subsequently transmitted to the kinase domain.

Although spectroscopic and crystallographic data have provided invaluable insights into the structure and dynamics of ligand binding to FixLH, a detailed and quantitative thermodynamic/conformational description of signal initiation/propagation within the PAS heme domain has not yet been elucidated (*13*−*19*). This is due, in part, to the fact that no published work has accessed the temporal evolution of the thermodynamics associated with the signal, or detected intermediates in the intradomain signaling process. This situation results from limitations on methodologies so far applied to these proteins. For example, optical spectroscopies directly probe the electronic structure of a specific chromophore (in this case the heme sensor), whereas changes in global protein structure that do not directly affect the chromophore may not be detected. Likewise, the crystal structure is limited to probing static conformations associated with a particular ligation state. Crystallography has yet to probe transient conformational changes required for transitions between states or to structurally define intermediates associated with the intradomain signal.

In this work, we overcome such limitations by employing transient optical and photothermal methods in solution. We report results from photoacoustic calorimetry (PAC) measurements after heme ligand photolysis that simulates the "signal trigger" in FixLs. By using these complementary methods, it is possible to directly probe global structural and thermodynamic changes taking place on an approximately nanosecond to microsecond time scale during the temporally evolving signal within the *Bj*FixL sensing domain. PAC has successfully been applied in previous studies of ligand photodissociation from iron porphyrin model systems, as well as to a variety of heme proteins (*20*, *21*). Notably, this marks the first PAC results on a heme sensing/signaling domain. In all of the previous naked heme/heme protein studies, it has been optical spectroscopies that have provided information concerning changes associated solely with the heme chromophore, whereas PAC reveals the magnitudes and time scales (i.e., kinetics) of global volume and enthalpy changes after a photoinitiated reaction. Thus, events that could not be detected by optical or vibrational techniques were detected and characterized using PAC.

Photoacoustic calorimetry has also been previously employed in probing volume and enthalpy changes in two sensing proteins having PAS-type folds. Terazima and coworkers (*22*) have studied conformational changes after photoexcitation of the hydroxycinnamic acid active site associated with photoactive yellow protein (PYP). It was determined that photoexcitation of the ground state produced a red-shifted intermediate within 2 ns, demonstrating a corresponding volume contraction of ∼7 mL/mol. The enthalpy associated with this transition was found to be 160 kJ/mol. Interestingly, this volume contraction was found to be temperature-dependent. More recently, a PAC study on the LOV1 domain from the "Phot" protein, which is a blue light receptor in *Chlamydomonas reinhardtii*, was reported (*23*). It was found that a volume contraction also occurred during formation of the initial photointermediate (approximately −1.5 mL/mol) with an additional volume contraction of ∼9 mL/mol for subsequent decay to the covalent FMN−Cys57 species. The volume and enthalpy changes determined by PAC for these two PAS domain proteins have provided novel insights into the conformational dynamics of signaling that have not been observed using optical methods.

In this report, we present results of PAC and transient absorption studies of conformational changes associated with photodissociation of carbon monoxide from two forms of *Bj*FixLH. The first form is our construct of the complete PAS heme domain, *Bj*FixLH$_{140-270}$, which begins with Thr140 and ends with Gln270. To begin determining the experimental importance of the size or extensiveness of the specific heme domain employed, we have also examined a second, truncated, form (*Bj*FixLH$_{151-256}$). *Bj*FixLH$_{151-256}$ is truncated at both ends of the polypeptide chain compared to *Bj*FixLH$_{140-270}$, with 11 amino acid residues deleted from the N-terminus and 14 amino acid residues deleted from the C-terminus.

MATERIALS AND METHODS

Fe^{3+} tetrakis(4-sulfonatophenyl)porphine [Fe(III)4SP] was purchased from Porphyrin Products Inc. and sodium dithionite from Fisher. CO gas was obtained from Matheson.

Protein Preparation. Detals of *Bj*FixLH production, isolation, and purification along with purity assessments are given elsewhere (*24*). Briefly, the gene encoding the full-length *Bj*FixL protein was a gift from H. Hennecke (ETH, Zurich, Switzerland). It was cloned into pET24a+ and expressed in *Escherichia coli* strain BL21(DE3). Expressed proteins were purified by ion-exchange and gel filtration chromatography and were assessed for purity using UV−visible spectroscopy (GBC Scientific, Cintra 40), SDS−PAGE, and MALDI-TOF mass spectrometry (Voyager DE). Yields of protein at least 95% pure were approximately 30 mg/L.

Samples for Optical and Photothermal Measurements. Samples for the transient absorption/PAC measurements were prepared by diluting the protein into 50 mM Tris buffer (pH 7.5) containing 50 mM NaCl to a final concentration of ∼10 μM. To obtain the deoxy form of *Bj*FixL, samples were sealed in a 1 cm quartz cuvette with a septum cap, purged with Ar, and reduced by adding several microliters of a buffered solution of sodium dithionite. The corresponding CO adducts were prepared by saturating deoxy samples with CO gas. Because of the lower stability of the *Bj*FixLH$_{140-270}$ protein toward degradation, measurements were performed with freshly prepared samples. Formation of deoxy and CO-bound forms of both proteins was monitored by UV−vis spectroscopy. Steady-state UV−vis spectra were recorded using a double-beam spectrophotometer (Shimadzu, UV-2401-PC).

Transient Absorption Measurements. The instrumentation used to perform the transient absorption measurements consists of a probe beam (150 W Xe arc lamp, Thermo-Oriel) passing through a 1/8M single monochromator (MC1-02, Optometrics USA) and centered on the sample housed in a temperature-controlled cuvette holder (Flash 200, Quantum Northwest). The light emerging from the sample is then focused on the slit of a second monochromator (1/4 M H-10, Jobin Yvon) and detected by a PMT (H6780, Hamamatsu) coupled with an amplifier (70710, Thermo-Oriel). The signal is then digitized using a 4 GHz transient digitizer (TDS 7404, Tektronix). The photochemistry was initiated by a 532 nm pulse from a Nd:YAG laser (Minilite I, Continuum) with a 7 ns pulse width and a 1 Hz repetition rate.

Photoacoustic Calorimetry. The instrumentation for photoacoustic calorimetry has been described in detail elsewhere (*20*, *25*). The sample contained in a 1 cm × 1 cm quartz cuvette was situated in a temperature-controlled cuvette holder (Flash 200PAS, Quantum Northwest), and a photoacoustic detector (1 MHz transducer, Panametrics V103) was pressed against the side of the cuvette. The connection between the cuvette and detector was facilitated by a thin layer of vacuum grease. The photoacoustic signal was amplified by a ultrasonic preamplifier (Panametrics 5662) and recorded using an NI 5102 oscilloscope (15 MHz) controlled by Virtual Bench-Scope software (National Instruments). Typically, 30−50 laser pulses were averaged per trace in the temperature range from 16 to 35 °C. Excitation was provided by a frequency-doubled Nd:YAG laser (532 nm, 7 ns pulse, <100 μJ/pulse, 1 Hz repetition rate) (Minilite I, Continuum). Fe(III)4SP was used as a calorimetric reference compound for the photothermal measurements. The absorbance of the reference matched the absorbance of the sample at the excitation wavelength ($A_{532} \sim 0.3$).

The theory and application of PAC have been reviewed in detail elsewhere (*20*, *25*). Briefly, at least two processes contribute to the photoacoustic wave generated after photoexcitation: the heat released during the reaction and corresponding structural changes (including bond cleavage and/or formation, electrostriction, etc.). Thus, the acoustic signal can be described as

$$S_{\mathrm{sam}} = KE_{\mathrm{a}}(\Delta V_{\mathrm{th}} + \Delta V_{\mathrm{con}}) \quad (1)$$

where K is an instrument response parameter, E_{a} is the number of Einsteins absorbed by the sample, and ΔV_{th} and ΔV_{con} represent the thermal and conformational contribution to the solution volume change, respectively. The thermal volume change can be expressed as

$$\Delta V_{\mathrm{th}} = Q(\beta/C_p\rho) \quad (2)$$

where Q is the amount of heat released to the solvent, β is the coefficient of thermal expansion of the solvent (K^{-1}), C_p is the heat capacity (cal g^{-1} K^{-1}), and ρ is the density (g mL^{-1}). The instrument response parameter can be eliminated by employing a reference compound that promptly converts the energy of the absorbed photon, $E_{h\nu}$, into heat with a quantum yield of unity and which undergoes no conformational changes. The amplitude of the acoustic signal for the reference compound is then described as

$$S_{\mathrm{ref}} = KE_{\mathrm{a}}E_{h\nu}(\beta/C_p\rho) \quad (3)$$

The ratio of the sample signal to the reference signal (ϕ) gives the following expression

$$\phi_i E_{h\nu} = (S/R)E_{h\nu} = Q + \Delta V_{\mathrm{con}}/(\beta/C_p\rho) \quad (4)$$

Thus, a plot of $\phi_i E_{h\nu}$ versus the temperature-dependent $C_p\rho/\beta$ term gives a straight line with a slope equal to ΔV_{con} and an intercept equal to the released heat (Q).

The acoustic transducer is sensitive to the amplitude of an acoustic wave as well as to its temporal profile. For example, if a photoinitiated process involves a two-step sequential decay process on the time scale of the transducer resolution (~50 ns to ~10 μs), the individual contributions of ΔV_{con} and Q for each kinetic process can be resolved. The observed time-dependent acoustic signal $E(t)_{\mathrm{obs}}$ is produced by the convolution of an instrument response function $T(t)$ (the reference acoustic wave) with a time-dependent function describing the decay processes, $H(t)$:

$$E(t)_{\mathrm{obs}} = H(t) \times T(t) \quad (5)$$

where

$$H(t) = \phi_1 \exp(-\tau/t_1) + [\phi_2 k_2/(k_2 - k_1)][\exp(-\tau/t_1) - \exp(\tau/t_2)] \quad (6)$$

$T(t)$ can be independently determined from the reference compound. We have used Simplex parameter estimation software developed in our laboratory to obtain the parameters ϕ_i and t_i. Deconvolution of the signal involves estimation of the parameters ϕ_i and t_i for $H(t)$ and a convolution of the estimated $H(t)$ function with the $T(t)$ function. The parameters are varied until the estimated $E(t)$ fits $E(t)_{\mathrm{obs}}$ (which is evident from the reduced χ^2 value). Processes occurring faster than roughly 50 ns cannot be resolved, but the integrated enthalpy and volume changes can be quantified from the amplitude of the acoustic wave.

RESULTS

Figure 1 displays the steady-state absorption spectra for the complete heme domain of *Bj*FixLH$_{140-270}$. The Soret peak of the met (Fe^{3+}) form is centered at 395 nm and upon heme reduction undergoes a bathochromic shift to 434 nm. The deoxy form exhibits a broad Q-band centered at 565 nm that is characteristic of a five-coordinate high-spin ferrous heme. Upon addition of CO, the absorption spectrum exhibits a Soret band at 425 nm and α and β bands at 543 and 575 nm, respectively. UV−vis spectra obtained for *Bj*FixLH$_{151-256}$ were essentially identical to those obtained for *Bj*FixLH$_{140-270}$ (data not shown). The observed spectral features correspond to those reported previously for the *Bj*FixLH and FixL heme domains from *S. meliloti* (*18*, *19*, *24*).

Rodgers et al. (*26*) have reported that for *S. meliloti* FixLH, photolysis of the heme−CO bond occurs with an overall quantum yield of 0.86 (i.e., quantum yield for CO diffusing from the heme binding pocket). Photoexcitation of the heme−CO bond leads to the formation of a geminate pair with the Fe−CO bond broken and CO remaining in the distal heme pocket. Subsequently, the ligand either rebinds on a

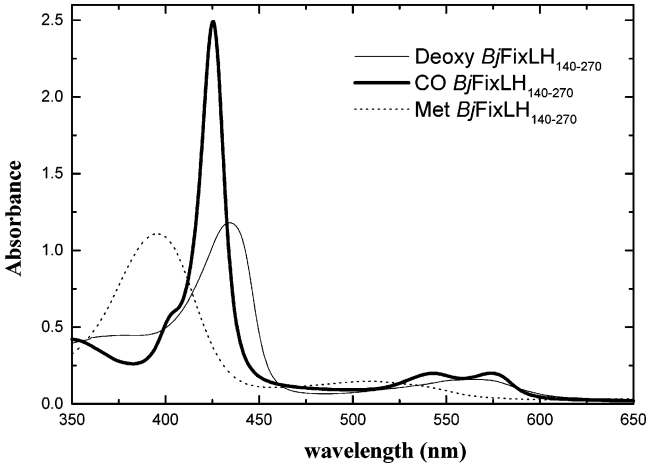

FIGURE 1: Equilibrium UV−vis spectra of *Bj*FixLH$_{140-270}$ in the met (dashed line), deoxy (thin line), and CO-bound forms (thick line). The sample concentration was 10 μM in 50 mM Tris buffer (pH 7.5) containing 50 mM NaCl at pH 7.5 and 22 °C.

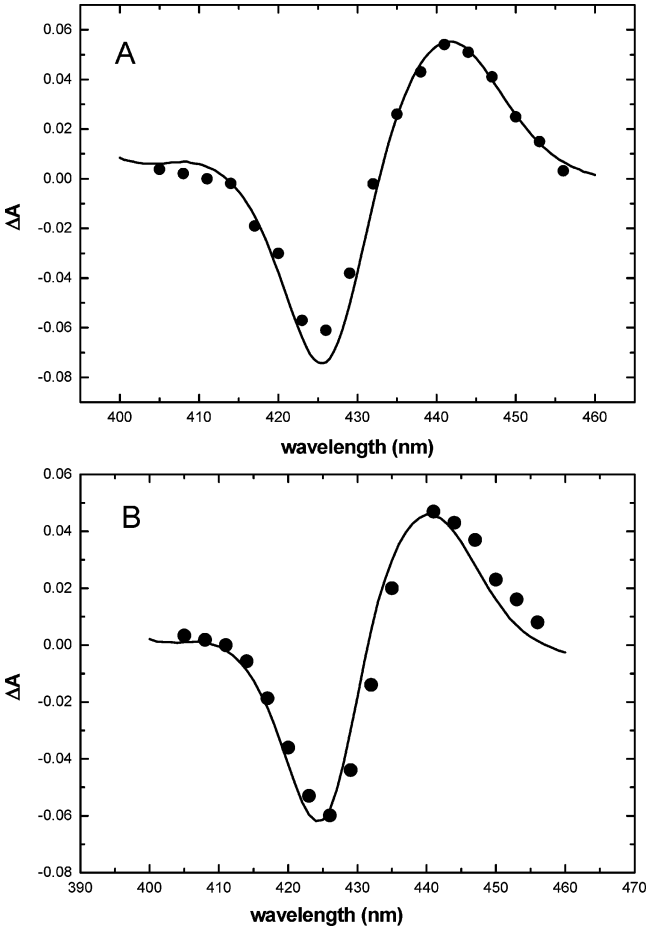

FIGURE 2: Transient difference spectrum of *Bj*FixLH$_{140-270}$ (A) and *Bj*FixLH$_{151-256}$ (B). Points represent data obtained 5 μs after CO photodissociation. The solid line is the steady-state difference spectrum (deoxy protein minus CO-bound protein). The transient and steady-state spectra are normalized to the same absorbance at 440 nm to better show the similarity in shape between the transient and the steady-state difference spectrum. Sample conditions: ~10 μM *Bj*FixLH, 50 mM Tris (pH 7.5), 50 mM NaCl, and 1 mM CO at 22 °C.

picosecond to nanosecond time scale or exits the protein. Figure 2 shows an overlay of the transient absorption spectra detected after CO photolysis from *Bj*FixLH$_{140-270}$ (trace A) and *Bj*FixLH$_{151-256}$ (trace B) together with the corresponding

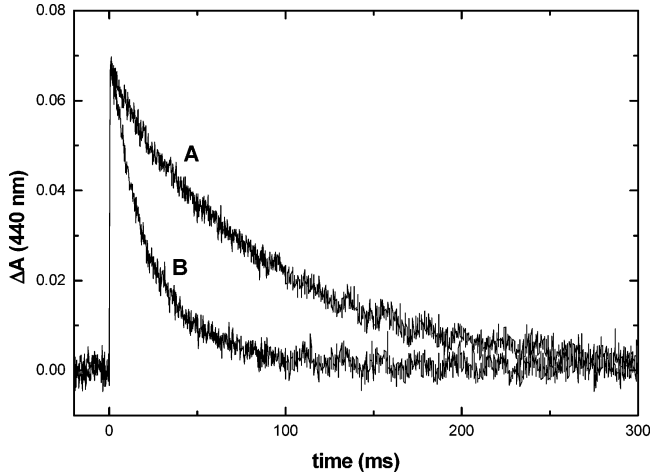

FIGURE 3: Transient absorption traces for rebinding of CO to *Bj*FixLH$_{140-270}$ (A) and *Bj*FixLH$_{151-256}$ (B) at 440 nm after photolysis. Sample conditions are the same as in Figure 2. The systematic oscillation with longer times is due to photomultiplier noise induced by the laser Q-switch.

steady-state difference spectra. The amplitudes of the transient spectra (points) were normalized to match the amplitudes of the steady-state spectra (line) at 440 nm to better illustrate similarities in the line shapes of the transient and steady-state difference spectra. For both *Bj*FixLH$_{140-270}$ and *Bj*FixLH$_{151-256}$, the amplitudes of the transient absorption spectra, upon CO photolysis, are roughly 50% of those of the steady-state difference spectra, suggesting a lower quantum yield than that obtained for *S. meliloti* FixLH. In addition, the transient spectra have the same line shape as the steady-state difference spectra (deoxy *Bj*FixLH minus CO-bound *Bj*FixLH), suggesting that the transient five-coordinate species formed after photolysis has an equilibrium heme pocket conformation.

Single-wavelength kinetic traces for rebinding of CO to both heme domains measured at 440 nm are shown in Figure 3. All rate measurements were carried out under pseudo-first-order conditions with CO in a large excess. Traces were fit to a single-exponential decay. The CO rebinding rate constants were found to be 10.2 ± 0.3 s^{-1} for *Bj*FixLH$_{140-270}$ and 17.3 ± 0.1 s^{-1} for *Bj*FixLH$_{151-256}$ at 18 °C. From the temperature dependence of the CO rebinding rate constants, activation energies were determined to be 14.7 ± 1.2 and 16.4 ± 1.9 kcal/mol for *Bj*FixLH$_{140-270}$ and *Bj*FixLH$_{151-256}$, respectively. The Arrhenius plots are shown in Figure 4. It is worth noting that the activation parameters are significantly smaller than those reported by Rodgers et al. for rebinding of CO to the full-length protein of *S. meliloti* (E_a = 54 kcal/mol) (*26*).

Volume and enthalpy changes associated with CO photodissociation were determined from PAC measurements. An overlay of the acoustic trace for photolysis of CO from *Bj*FixLH$_{140-270}$ with the corresponding reference trace at 35 °C (Figure 5) shows a phase shift of the sample acoustic wave relative to the reference wave. Such shifts indicate the presence of kinetic processes occurring between <50 ns and ~10 μs. The lifetimes (τ_i) and amplitudes (ϕ_i) for the individual processes were obtained by deconvolution of the sample acoustic signals as described in Materials and Methods. Satisfactory fits of the sample signals for *Bj*FixLH$_{140-270}$ were achieved using a double-exponential

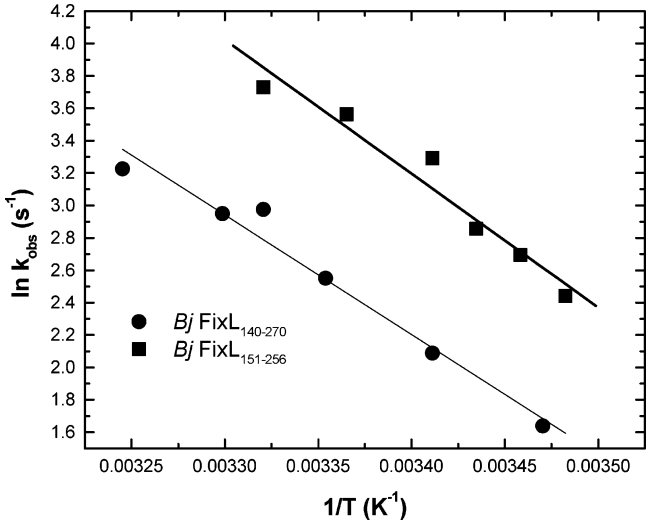

FIGURE 4: Arrhenius plot for CO recombination to *Bj*$FixLH_{140-270}$ and *Bj*$FixLH_{151-256}$. Data are from the temperature dependence of the transient absorption traces described in Figure 3.

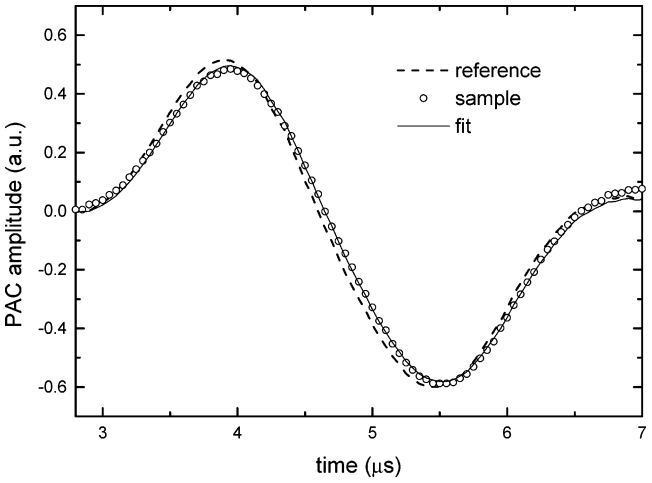

FIGURE 5: Photoacoustic traces for photodissociation of CO from *Bj*$FixLH_{140-270}$ and the corresponding reference compound at 35 °C. The absorbance of the sample and reference at the excitation wavelength (532 nm) was 0.25. Sample conditions were as described in the legend of Figure 2.

decay scheme. The first decay occurs faster than the resolution of our instrument (τ_1 < 50 ns), and the second has a lifetime (τ_2) of ~150 ns in the temperature range of 15−35 °C. According to eq 4, the volume and enthalpy changes for each process can be determined by plotting a ratio of the sample amplitude to the reference amplitude, scaled to the energy of the laser pulse at 532 nm ($\phi_i E_{h\nu}$) versus a temperature-dependent factor, $C_p\rho/\beta$. Figure 6 displays plots of $\phi_i E_{h\nu}$ versus $C_p\rho/\beta$ for both phases for *Bj*$FixLH_{140-270}$. The slope of the linear fits corresponds to the volume change per mole of photons absorbed and the intercept to the heat released to the solvent. For reactions with a quantum yield (Φ) of <1, the reaction volume change for each process is obtained using

$$\Delta V = \Delta V_{con}/\Phi \quad (7)$$

and ΔH for the reaction for the fast phase (τ < 50 ns) is calculated using

$$\Delta H = (E_{h\nu} - Q)/\Phi \quad (8)$$

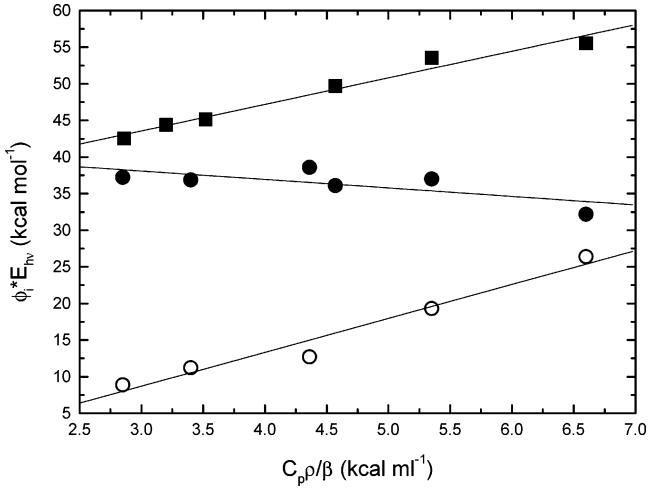

FIGURE 6: Plot of $\phi_i E_{h\nu}$ vs $C_p\rho/\beta$ for fast phase (●) and slow phase (○) of photodissociation of CO from *Bj*$FixLH_{140-270}$ and for the single observed combination phase from $BjFixLH_{151-256}$ (■). Conditions were as described in the legend of Figure 2.

Table 1: Summary of PAC Results for *Bj*$FixLH_{140-270}$ and *Bj*$FixLH_{151-256}$[a]

	fast phase (<50 ns)		slow phase		
	ΔH (kcal/mol)	ΔV (mL/mol)	ΔH (kcal/mol)	ΔV (mL/mol)	τ (ns)
2-MeIm(Fe)4SP[b]	17 ± 3	21.1 ± 0.7	−	−	−
myoglobin[c]	7.4 ± 2.0	−1.7 ± 0.6	5.5 ± 1.2	15.5 ± 0.5	700
Bj$FixLH_{140-270}$	14 ± 3	−1.4 ± 0.8	6.0 ± 3.5	5.3 ± 0.7	150
Bj$FixLH_{151-256}$	25 ± 4.0	4.9 ± 0.4	−	−	−

[a] PAC results for a heme model complex and CO-bound horse heart myoglobin are also included. [b] From ref *36*. [c] Data for horse heart myoglobin in 100 mM Tris buffer (*27*, *29*).

The enthalpy change for the subsequent processes is related to the heat deposited to the solvent by $\Delta H = -Q/\Phi$. To calculate reaction volume and enthalpy changes, we used a Φ of 0.86 determined by Rodgers et al. (*19*) (although, as noted above, this value may be somewhat smaller for the samples measured in this study). The volume and enthalpy changes determined for each process are summarized in Table 1 together with values determined previously for myoglobin and a model heme compound [2-methylimidazole Fe(II)4SP]. Lifetimes for the slow phase process over a temperature range of 15−35 °C were determined to be ~150 ns and do not exhibit significant temperature dependence, possibly due to the very low activation energy.

Figure 7 displays the corresponding overlay of an acoustic trace for photodissociation of CO from the truncated *Bj*$FixLH_{151-256}$ domain and a reference trace measured at 35 °C. Unlike the case for the full-length heme domain, no phase shift is observed indicating no volume and/or enthalpy changes take place between ~50 ns and ~10 μs. On the other hand, the sample trace exhibits a smaller amplitude than the reference trace, indicating the presence of volume and enthalpy changes occurring within <50 ns of CO photodissociation. A plot of $\phi_i E_{h\nu}$ versus $C_p\rho/\beta$ is provided in Figure 6, and the $\Delta V/\Delta H$ values are also summarized in Table 1 and discussed below.

DISCUSSION

To probe intradomain signaling in the FixL class of PAS domain heme oxygen sensors, we have characterized the

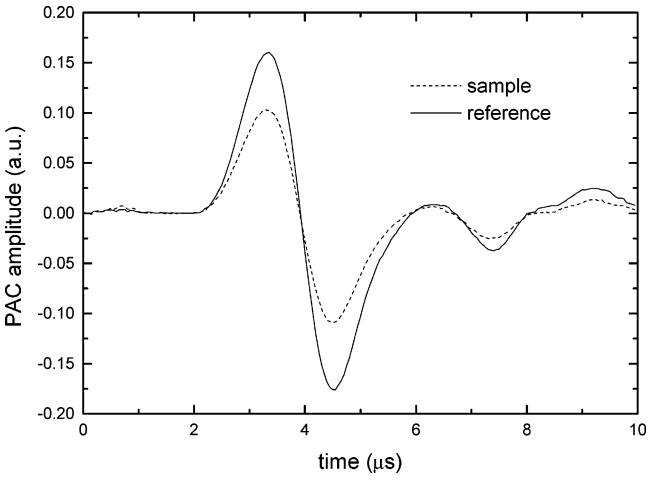

FIGURE 7: Photoacoustic traces for photodissociation of CO from *Bj*FixLH$_{151-256}$ and the corresponding reference trace. The absorbance of the sample and reference at the excitation wavelength (532 nm) was 0.2. Conditions: 50 mM Tris (pH 7.5), 50 mM NaCl, and 1 mM CO at 35 °C.

thermodynamic and kinetic parameters associated with ligand binding in two forms of the FixL heme domain from *B. japonicum*. *Bj*FixLH$_{140-270}$ contains the most extensive PAS core, composed of a five-stranded antiparallel β barrel and a central α helix. In contrast, *Bj*FixLH$_{151-256}$ is a truncated domain, missing 11 amino acid residues on the N-terminal end and 14 residues on the C-terminal end, but retaining heme binding and other essential structural components of a functional heme−PAS core. Transient absorption results demonstrate that the truncations do not significantly affect the conformation of the heme pocket after CO photolysis or the rate of ligand recombination. The transient absorption spectra after ligand photodissociation are nearly identical for both forms of the protein and have a line shape that can be superimposed with the corresponding equilibrium difference spectrum. These results suggest that upon ligand photodissociation for both proteins, the heme and surrounding protein environment relax to the equilibrium unliganded conformation in less than ~5 μs.

Previously, Liebl et al. (*27*) using femtosecond spectroscopy to study photodissociation of ligand from *Bj*FixLH reported small spectral changes taking place within the first 200 fs and the absence of additional spectral evolution between ~1 ps and 4 ns. In addition, those authors observed that the absorption spectrum of the transiently formed deoxy species was distinct from that of the equilibrium deoxy form and that this difference persisted up to the time limit of their instrumentation (~4 ns). Those results indicate that upon photolysis an intermediate is formed with an unrelaxed heme pocket, which decays with a rate faster than ~5 ms.

The single-wavelength transient absorption data presented here show that ligand recombination to the five-coordinate heme *Bj*FixLH$_{140-270}$ occurs with a rate constant of ~10 s^{-1} at 18 °C and under 1 atm of CO (i.e., 1 mM solution concentration) (vide supra). Under identical conditions, we observed a slightly faster rate constant (~17 s^{-1}) for rebinding of CO to *Bj*FixLH$_{151-256}$. These pseudo-first-order rate constants are similar to rate constants previously reported for rebinding of CO to the *S. meliloti* FixL heme domain (k_{obs} = 25.8 s^{-1} at 24.5 °C) (*1*, *18*) and from *B. japonicum* (k_{obs} = 5 s^{-1} at 25 °C) (*18*). Similarity in CO rebinding rates as well as the fact that the transient difference spectra are superimposable with the equilibrium difference spectra for both *Bj*FixLH$_{140-270}$ and *Bj*FixL$_{151-256}$ demonstrates that changes in the heme pocket that are coupled to ligand photodissociaiton and subsequent rebinding are not affected by the truncation at the N- and C-terminal ends of the heme domain.

Before the PAC data on *Bj*FixLH are interpreted, it is instructive to consider previous PAC studies on myoglobin (Mb). Peters and collaborators (*21*, *28*) used PAC to determine volume and enthalpy profiles for dissociation of CO from myoglobin. Those studies revealed that ligand dissociation is characterized by a small endothermic (ΔH = 6 kcal/mol) volume contraction (ΔV = −1.9 mL/mol) (*28*). On longer time scales, an intermediate with a lifetime of ~800 ns (at 20 °C) was identified which had not been previously observed by optical methods. It was reported that the decay of the intermediate is coupled to a volume expansion of ~13 mL/mol. The initial contraction was associated with the disruption of a salt bridge between Arg45 and the heme 6-propionate side chain and the subsequent 800 ns phase with the reformation of this salt bridge. Recently, the Terazima group (*29*, *30*) extended the study of ligand dissociation from myoglobin to the picosecond time scale using transient grating spectroscopy. In agreement with the previously reported results, they observed a 700 ns kinetic event but attributed this phase to escape of the ligand from the protein to the solvent or possibly protein relaxation after ligand escape.

Similar to those CO−Mb studies, our PAC studies of *Bj*FixLH$_{140-270}$ reveal the presence of two kinetic processes following ligand photodissociation. Within 50 ns, a small contraction of −1.4 mL/mol is observed, and this phase is followed by a volume expansion of 5.3 mL/mol with a lifetime of ~150 ns (which are ~0.003 and ~0.013% of the total protein volume, respectively, assuming a volume for the full length heme domain of ~25130 Å^3/molecule obtained from the crystal structure). It should be noted that the volume change observed for these two phases is quite distinct from the overall volume change calculated from the crystal structure using QSAR (Quantitative Structure Activity Relationship) in HyperChem. The volume change calculated from the crystal structures is essentially ΔV_{vdw} and does not include any solvent interaction terms. The total volume change calculated in this way ($\Delta V_{vdw} = V_{CO} + V_{deoxyFixL} - V_{COFixL}$, where $V_{deoxyFixL}$ and V_{COFixL} are calculated from the crystal structures and V_{CO} is determined from HyperChem) is ~48 mL/mol. It is unclear to what extent ΔV_{vdw} obtained from the crystal structures contributes to the overall ΔV obtained from the PAC measurements since ΔV_{vdw} does not contain any solvation parameters and is calculated from static structures, whereas the PAC data involve an intermediate.

The similarity in the magnitude of the initial volume contraction between *Bj*FixLH$_{140-270}$ and CO−Mb suggests that the origin of the contraction may be similar in both proteins. In the case of myoglobin, CO photodissociation and relaxation of the heme to the equilibrium high-spin electronic configuration take place in <350 fs (*31*, *32*) and the photoproduct attains the equilibrium deoxy conformation after ~3 ns (*33*). A detailed characterization of the structural differences within the heme binding pocket of FixLH from *S. meliloti* in the presence and absence of carbon monoxide

has been provided by resonance Raman (*19*, *34*) and EXAFS spectroscopy (*34*). Those studies showed that the Fe−CO and Fe−N_{im} bond distances in FixL and myoglobin are basically identical, although the Fe−C═O angle in FixLH is more linear than in myoglobin. Using transient resonance Raman spectroscopy, Rodgers et al. (*19*) identified a transient intermediate after CO photodissociation. Relative to the relaxed deoxy FixLH, the intermediate exhibits a shorter Fe−His bond, and such bond compression was proposed to provide sufficient energy to drive protein conformational changes.

Thus, the similar initial volume contractions identified in myoglobin and *Bj*FixLH arise from changes in their respective heme domains that are coupled to Fe−CO bond cleavage, the low-spin to high-spin heme transition, and possibly a salt bridge disruption. We consider these possibilities in more detail. Previous high-pressure studies have suggested that the low-spin to high-spin change for transition metal centers is accompanied by a volume increase of ∼12 mL/mol, whereas bond fission reactions have characteristic volume increases of ∼5 mL/mol (*35*). Since the initial events in the photolysis of CO from the heme iron of *Bj*FixLH include a low-spin to high-spin transition as well as CO−Fe bond cleavage, a total volume increase of ∼17 mL/mol might be expected (that is, if the protein behaves simply as a heme "solvent"). The fact that the volume change observed for processes taking place in <50 ns is approximately −1.4 mL/mol indicates that a volume decrease takes place that is larger than the expected volume increase due to the heme photochemistry (i.e., $-1.4\ \text{mL/mol} \sim \Delta V_{\text{LS-HS}} + \Delta V_{\text{Fe-CO}} + \Delta V_{\text{protein}}$). This places the magnitude of $\Delta V_{\text{protein}}$ on the order of approximately −18.4 mL/mol.

What can account for this volume change? One possibility results from considering that this value is similar to that expected for electrostriction of water around a newly created charge, a contraction of ∼12−15 mL/mol. This similarity to $\Delta V_{\text{protein}}$ for the *B*jFixLH−CO species suggests that cleavage of the CO−Fe bond results in disruption of a peripheral salt bridge interaction, allowing for a more solvent-exposed charge (*34*) and accompanying electrostriction.

The initial contraction is also endothermic, with an enthalpy change of 14.1 ± 3.5 kcal/mol. This value is similar to the enthalpy of Fe−CO bond cleavage, which has been determined to be ∼17 kcal/mol for myoglobin (*26*) and for the heme model compound (2-methylimidazol)Fe(II)4SP (*36*). Thus, there are two processes that contribute for the initial enthalpy and volume changes. At this point, we also note that the transient intermediate identified using resonance Raman spectroscopy is not likely to be resolved by PAC due to an undetectably short lifetime (<50 ns) or to the fact that compression of the Fe−His bond may not be coupled to significant volume and/or enthalpy changes.

For *Bj*$FixLH_{140-270}$, the initial contraction is followed by a subsequent 150 ns phase. This longer time phase is associated with a volume expansion of 5.3 ± 0.8 mL/mol and an enthalpy change of 6.0 ± 3.5 kcal/mol. Several processes can contribute to the observed positive volume change: migration of CO through the protein matrix, escape of CO into the surrounding solvent, and/or protein conformational changes. Release of CO to the solvent (aqueous buffer in this case) is expected to have a positive volume change since fragmentation reactions are in general coupled to the increase in overall volume (*37*). In addition, the enthalpy change of 6.0 ± 3.5 kcal/mol determined for the 150 ns phase is close to the value for CO solvation, which has been estimated to be 2.6 kcal/mol (*38*). Therefore, the volume and enthalpy changes associated with the 150 ns phase are consistent with those expected for the escape of CO from the protein matrix and concomitant solvation.

Interestingly, a phase comparable to the 150 ns phase is missing in the case of *Bj*$FixLH_{151-256}$. PAC data for photodissociation of CO from *Bj*$FixLH_{151-256}$ show only one phase, and that occurs within ∼50 ns of photolysis. However, for *Bj*$FixLH_{151-256}$, the observed volume expansion (ΔV = 4.2 ± 0.3 mL/mol) for this single, <50 ns phase represents the physical processes that are the sum of the volume change for the initial contraction and 150 ns expansion found for release of CO from *Bj*$FixLH_{140-270}$. That is, for *Bj*$FixLH_{140-270}$, $\Delta V_{\text{total}} \sim -1.4\ \text{mL/mol} + \sim 5.3\ \text{mL/mol} \sim 3.9\ \text{mL/mol}$ compared to a ΔV of 4.2 ± 0.3 mL/mol for *Bj*$FixLH_{151-256}$. Likewise, the enthalpy change of 25 kcal/mol for *Bj*$FixLH_{151-256}$ is only slightly greater than the sum of the enthalpy changes of the fast and slow phases observed for *Bj*$FixLH_{140-270}$. Consequently, we consider it likely that the truncation of 11 amino acid residues at the N-terminus and 14 amino acid residues at the C-terminus of the *Bj*FixL PAS heme domain causes changes associated with the protein surface that accelerate the release of ligand from the protein and/or change salt bridge interactions.

With a view to attributing these PAC changes to a specific structural feature, we note that changes in salt bridges have been previously implicated in PAC studies of Mb (*21*), and are also thought to contribute to signaling in LOV, a non-heme PAS protein. Crosson et al. (*39*) proposed that in the LOV family of PAS domain proteins a surface salt bridge plays an important role in the interaction between the signaling LOV domain and an interaction partner. They suggested that the breaking or formation of the salt bridge changes the conformational flexibility of the LOV domain and thereby modulates interdomain interactions.

One possibility for *Bj*$FixLH_{140-270}$ is that dynamics associated with a similar surface salt bridge could contribute to PAC results. Such a salt bridge exists in both FixLH and *Ec*Dos. In *Bj*FixLH, this salt bridge is formed between Glu182 and Arg227. The thermodynamic parameters determined by PAC are consistent with a model in which the release of ligand from *Bj*FixLH is coupled to the disruption of this salt bridge, which in turn changes the overall charge distribution on the protein surface (thus accounting for the fast phase volume contraction). Such changes in charge distribution could also change interactions between the FixL sensor and kinase domains, thereby influencing interdomain signal transduction as in LOV. The heme communicates with the surface area of *Bj*FixLH that includes the Glu182−Arg227 salt bridge, as shown by our unpublished work (*40*) in which the fluorescence of Trp178, a structural neighbor to the salt bridge, changes upon heme ligation. We speculate that heme−surface communication occurs through a pathway involving hydrophobic residues similar to that proposed for the LOV domains (*39*). The residues participating in such a connecting pathway are shown in Figure 8.

In contrast to these solution results, it is interesting that crystal structures of the CO-bound and deoxy forms of *Bj*FixLH show only small perturbations in the Trp178−

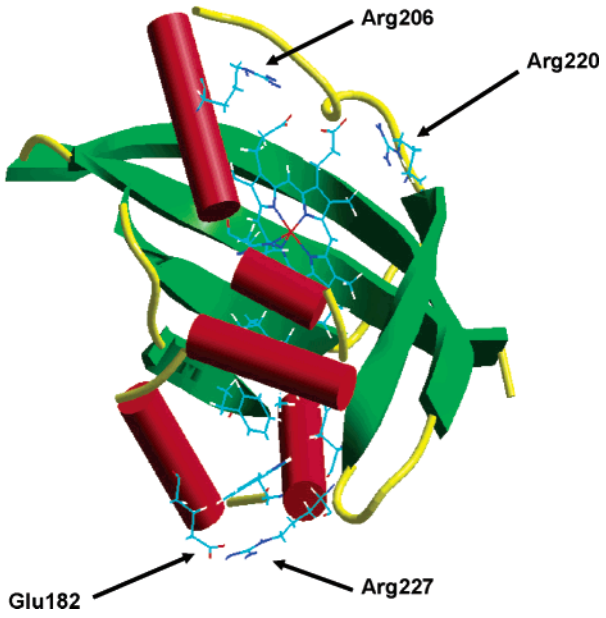

FIGURE 8: Ribbon diagram of the FixL heme domain X-ray crystal structure in the ligand free-state (PBD entry 1XJ4). The heme cofactor and hydrophobic residues proposed to connect the surface salt bridge (Trp178, Phe168, Phe176, Ile157, and Leu191) are shown as well as the salt bridge formed by Glu182 and Arg227. The heme propionate−Arg206/Arg220 interactions are also shown.

Glu182−Arg227 area, which would argue against salt bridge disruption as the source of the volume contraction (*41*). However, again, this is similar to the case found in Mb where the structural perturbations observed in the Mb crystal structure between Arg45 and the heme propionate 6 are also small, but wherein mutation of the Arg residue significantly reduced the observed volume contraction (*21*) in solution measurements. Thus, for both Mb and *Bj*FixLH, salt bridge disruption may be transient or simply does not occur within the crystallized forms of each protein, perhaps as a consequence of crystal packing forces.

An alternative possibility to account for the PAC results involves changes in the position of the Arg206 side chain (Figure 8). A recent crystallographic study by Key and Moffat (*41*) of the deoxy and CO-bound forms of a *Bj*FixL heme domain showed increased disorder of Arg206 upon CO binding. Arg206 has been proposed to compensate for the charge on heme propionate 7 due to release of Arg220 (Figure 8) that rotates into the heme pocket upon oxygen binding (*42*, *43*). In the case of CO binding, the Arg220−heme propionate salt bridge remains intact but the increased heme planarity does shift the FG loop, resulting in Arg206 disorder. Increased solvent exposure (and accompanying electrostriction) of this Arg residue could also account for the observed volume decrease in our studies.

In any event, the photothermal data presented here have clearly revealed enthalpy and conformational changes after ligand photodissociation in both forms of the *Bj*FixL heme domain in solution. Although the precise nature of the volume contraction has not been elucidated, our results are the first quantitation of energetic and volumetric events that are associated with intradomain signal initiation, and likely with intradomain signal propogation, for any heme oxygen sensing or signaling protein. These results provide quantitative boundries as well for the kinetics of these conformational changes. In total, these studies provide the basis for a new framework from which to probe initiation and evolution of the signaling event in FixL.

ACKNOWLEDGMENT

We acknowledge use of the Protein Data Bank, operated by the Research Collaboratory for Structural Bioinformatics (http://www.rcsb.org/pdb/).

REFERENCES

1. Soderling, S. H., and Beavo, J. A. (2000) Regulation of cAMP and cGMP signaling: New phosphodiesterases and new functions, *Curr. Opin. Cell Biol. 12*, 174−179.
2. David, M., Daveran, M.-L., Batut, J., Dedieu, A., Domergue, O., Ghai, J., Hertig, C., Boistard, P., and Kahn, D. (1988) Cascade regulation of *nif* gene expression in *Rhizobium meliloti*, *Cell 54*, 671−683.
3. Anthamatten, D., and Hennecke, H. (1991) The regulatory status of the fixL- and fixJ-like genes in *Bradyrhizobium japonicum* may be different from that in *Rhizobium meliloti*, *Mol. Gen. Genet. 225* (1), 38−48.
4. Sciotti, M.-A., Chanfon, A., Hennecke, H., and Fischer, H.-M. (2003) Disparate oxygen responsiveness of two regulatory cascades that control expression of symbiotic genes in *Bradyrhizobium japonicum*, *J. Bacteriol. 185*, 5639−5642.
5. Mesa, S., Bedmar, E. J., Chanfon, A., Hennecke, H., and Fischer, H. M. (2003) *Bradyrhizobium japonicum* NnrR, a denitrification regulator, expands the FixLJ-FixK2 regulatory cascade, *J. Bacteriol. 185*, 3978−3982.
6. Gilles-Gonzalez, M. A., Ditta, G. D., and Helinksi, D. R. (1991) A haemoprotein with kinase activity encoded by the oxygen sensor of *Rhizobium meliloti*, *Nature 350*, 170−172.
7. Gilles-Gonzalez, M. A., and Gonzalez, G. (1993) Regulation of the kinase activity of heme protein FixL from the two-component system FixL/FixJ of *Rhizobium meliloti*, *J. Biol. Chem. 268*, 16293−16297.
8. Monson, E. K., Weinstein, M., Ditta, G. S., and Helinski, D. R. (1992) The FixL protein of *Rhizobium meliloti* can be separated into a heme-binding oxygen-sensing domain and a functional C-terminal kinase domain, *Proc. Natl. Acad. Sci. U.S.A. 89*, 4280−4284.
9. Lois, A. F., Ditta, G. S., and Helinski, D. R. (1993) The oxygen sensor FixL of *Rhizobium meliloti* is a membrane protein containing four possible transmembrane segments, *J. Bacteriol. 175*, 1103−1109.
10. Chan, M. K. (2001) Recent advances in heme-protein sensors, *Curr. Opin. Chem. Biol. 5*, 216−222.
11. Rodgers, K. R. (1999) Heme-based sensors in biological systems, *Curr. Opin. Chem. Biol. 3*, 158−167.
12. Taylor, B. L., and Zhulin, I. B. (1999) PAS domains: Internal sensors of oxygen, redox potential, and light, *Microbiol. Mol. Biol. Rev. 63*, 479−506.
13. Gong, W., Hao, B., Mansy, S. S., Gonzalez, G., Gilles-Gonzalez, M. A., and Chan, M. K. (1998) Structure of a biological oxygen sensor: A new mechanism for heme-driven signal transduction, *Proc. Natl. Acad. Sci. U.S.A. 95*, 15177−15182.
14. Gong, W., Hao, B., and Chan, M. K. (2000) New mechanistic insights from structural studies of the oxygen-sensing domain of *Bradyrhizobium japonicum* FixL, *Biochemistry 39*, 3955−3962.
15. Jain, R., and Chan, M. K. (2003) Mechanisms of ligand discrimination by heme proteins, *J. Biol. Inorg. Chem. 8*, 1−11.
16. Perutz, M. F., Paoli, M., and Lesk, A. M. (1999) Fix L, a haemoglobin that acts as an oxygen sensor: Signalling mechanism and structural basis of its homology with PAS domains, *Chem. Biol. 6*, R291−R297.
17. Miyatake, H., Mukai, M., Park, S.-Y., Adachi, S.-I., Tamura, K., Nakamura, H., Makamura, K., Tsuchiya, T., Iizuka, T., and Shiro, Y. (2000) Sensory mechanism of oxygen sensor FixL from *Rhizobium meliloti*: Crystallographic, mutagenesis and resonance Raman spectroscopic studies, *J. Mol. Biol. 301*, 415−431.
18. Gilles-Gonzalez, M. A., Gonzalez, G., Perutz, M. F., Kiger, L., Marden, M. C., and Poyart, C. (1994) Heme-based sensors, exemplified by the kinase FixL, are a new class of heme protein with distinctive ligand binding and autoxidation, *Biochemistry 33*, 8067−8073.

19. Rodgers, K. R., Lukat-Rodgers, G. S., and Barron, J. A. (1996) Structural basis for ligand discrimination and response initiation in the heme-based oxygen sensor FixL, *Biochemistry 35*, 9539−9548.
20. Mikšovská, J., and Larsen, R. W. (2003) Structure−function relationships in metalloproteins, in *Methods in Enzymology* (Marriott, G., and Parker, I., Eds.) Biophotonics Series, Vol. 360, Part A, pp 302−329, Academic Press, New York.
21. Westrick, J. A., Peters, K. S., Ropp, J. D., and Sligar, S. G. (1990) Role of the arginine-45 salt bridge in ligand dissociation from sperm whale carboxymyoglobin as probed by photoacoustic calorimetry, *Biochemistry 29*, 6741−6746.
22. Takeshita, K. Y., Imamoto, M., Kataoka, F., Tokunaga, F., and Terazima, M. (2002) Themodynamic and transport properties of intermediate states of the photocyclic reaction of photoactive yellow protein, *Biochemistry 41*, 3037−3048.
23. Losi, A., Kottke, T., and Hegemann, P. (2004) Recording of blue light-induced energy and volume changes within the wild-type and mutated phot-LOV1 domain from *Chlamydomonas reinhardtii*, *Biophys. J. 86*, 1051−1060.
24. Suquet, C., Savenkova, M., and Satterlee, J. D. (2005) Recombinant PAS-heme domains of oxygen sensing proteins: High level production and physical characterization, *Protein Expression Purif. 42*, 182−193.
25. Braslavsky, S. E., and Heibel, G. E. (1992) Time-resolved photothermal and photoacoustic methods applied to photoinduced processes in solution, *Chem. Rev. 92*, 1381−1410.
26. Rodgers, K. R., Tang, L., Lukat-Rodgers, G. S., and Wengenack, N. L. (2001) Insights into the signal transduction mechanism of RmFixL provided by carbon monoxide recombination kinetics, *Biochemistry 40*, 12932−12942.
27. Liebl, U., Bouzhir-Sima, L., Negrerie, M., Martin, J. L., and Vos, M. H. (2002) Ultrafast ligand rebinding in the heme domain of the oxygen sensors FixL and Dos: General regulatory implications for heme-based sensors, *Proc. Natl. Acad. Sci. U.S.A. 99*, 12771−12776.
28. Westrick, J. A., and Peters, K. S. (1990) A photoacoustic calorimetric study of horse myoglobin, *Biophys. Chem. 37*, 73−79.
29. Sakakura, M., Morishima, I., and Terazima, M. (2002) Structural dynamics of distal histidine replaced mutants of myoglobin accompanied with the photodissociation reaction of the ligand, *Biochemistry 41*, 4837−4846.
30. Sakakura, M., Morishima, I., and Terazima, M. (2001) The Structural Dynamics and Ligand Releasing Process after the Photodissociation of Sperm Whale Carboxymyoglobin, *J. Phys. Chem. B 105*, 10424−10434.
31. Martin, J. L., Migus, A., Poyart, Y., Lecarpentier, R., Astier, R., and Antonetti, A. (1983) Femtosecond photolysis of CO-ligated protoheme and hemoproteins: Appearance of deoxy species with a 350-fsec time constant, *Proc. Natl. Acad. Sci. U.S.A. 80*, 1973.
32. Franzen, S., Bohn, B., Poyart, C., and Martin, J. L. (1995) Evidence for sub-picosecond heme doming in hemoglobin and myoglobin: A time-resolved resonance Raman comparison of carbonmonoxy and deoxy species, *Biochemistry 34*, 1224.
33. Henry, E. R., Sommer, J. H., Hofrichter, J., and Eaton, W. A. (1983) Geminate recombination of carbon monoxide to myoglobin, *J. Mol. Biol. 166*, 443.
34. Miyatake, H., Mukai, M. l., Adachi, S., Nakamura, H., Tamura, K., Iizuka, Y., Strange, R. W., and Hasnain, S. S. (1999) Iron coordination structures of oxygen sensor FixL characterized by Fe K-edge extended X-ray absorption fine structure and resonance Raman spectroscopy, *J. Biol. Chem. 274*, 23176−23184.
35. Van Eldik, R., Asano, T., and Le Noble, W. J. (1989) Activation and Reaction Volumes in Solution. 2, *Chem. Rev. 89*, 549−688.
36. Miksovska, J., Norstrom, J., and Larsen, R. W. (2005) Thermodynamic Profiles for CO Photodissociation from Heme Model Compounds: Effect of Proximal Ligands, *J. Inorg. Chem. 44*, 1006−1014.
37. Schmidt, R. (1998) Interpretation of Reaction and Activation Volumes in Solution, *J. Phys. Chem. A 102*, 9082−9086.
38. Leung, W. P., Cho, K. C., Chau, S. K., and Choy, C. L. (1987) Measurement of the Protein−Ligand Bond Energy of Carboxymyoglobin by Pulsed Photoacoustic Calorimetry, *Chem. Phys. Lett. 141*, 220.
39. Crosson, S., Rajagopal, S., and Moffat, K. (2003) The LOV domain family: Photoresponsive signaling modules coupled to diverse output domains, *Biochemistry 42*, 2−10.
40. Miksovska, J., Ganley, J., Suquet, C., Satterlee, J. D., and Larsen, R. W. (2005) Insights into the Signaling Mechanism of FixL from Trp128 Fluorescence, *J. Inorg. Biochem.* (submitted for publication).
41. Key, J., and Moffat, K. (2005) Crystal Structures of Deoxy and CO-Bound *bj*FixLH Reveal Details of Ligand Recognition and Signaling, *Biochemistry 44*, 4627−4635.
42. Hao, B., Isaza, C., Arndt, J., Soltis, M., and Chan, M. K. (2002) Structure-based mechanism of O_2 sensing and ligand discrimination by the FixL heme domain of *Bradyrhizobium japonicum*, *Biochemistry 41*, 12952−12958.
43. Dunham, C. M., Dioum, E. M., Tuckerman, J. R., Gonzalez, G., Scott, W. G., and Gilles-Gonzalez, M. A. (2003) A distal arginine in oxygen-sensing heme-PAS domains is essential to ligand binding, signal transduction, and structure, *Biochemistry 42*, 7701−7708.

BI047369B